



# A Comparative Study of Physical Properties of Er and Yb Nanophase Ferrite for Industrial Application

Asmaa A. H. El-Bassuony<sup>1</sup>

Received: 26 August 2017 / Accepted: 21 December 2017 / Published online: 9 January 2018  
© Springer Science+Business Media, LLC, part of Springer Nature 2018

## Abstract

Nano ferrites  $\text{CuCr}_{0.3}\text{Er}_{0.03}\text{Fe}_{1.67}\text{O}_4$  and  $\text{CuCr}_{0.3}\text{Yb}_{0.03}\text{Fe}_{1.67}\text{O}_4$  were synthesized using standard ceramic technique. X-ray diffraction (XRD) patterns confirmed that the samples had cubic spinel structures. The average crystallite sizes of Er and Yb samples were in the range of 104.2–100 nm. The morphology analyses using field emission scanning electron microscopy (FESEM), high-resolution transmission electron microscopy (HRTEM) and atomic force microscopy (AFM) confirmed that the samples were in the nanoscale range. The compositional analyses using energy-dispersive x-ray (EDX) showed the atomic percentage (at.%) and weight percentage (wt%) of the investigated samples. The magnetic properties were carried out at room (300 K) and at low (100 K) temperatures magnetic hysteresis loop. The data showed that Er sample had higher saturation magnetization ( $M_s$ ) and lower coercivity ( $H_c$ ) than that of Yb sample suggesting that Er sample can be applied in magnetic applications. Moreover, Er sample had higher dielectric constant ( $\epsilon'$ ), dielectric loss ( $\epsilon''$ ) and dielectric loss tangent ( $\tan \delta$ ) than that of Yb sample. However, Yb sample had higher resistivity than that of Er sample suggesting that Yb sample can be applied in electrical applications.

**Keywords** Rare earth · FESEM · HRTEM · AFM · Magnetic properties · Electrical properties

## 1 Introduction

Ferrites can be introduced by the chemical formula  $AB_2O_4$ , where  $A$  and  $B$  denote metal cations on tetrahedral ( $A$ ) and octahedral ( $B$ ) sites, respectively. Rare earth ions having unpaired 4f electrons and the strong spin-orbit coupling pays more attention in many technological applications [1]. Many researchers have been attracted to substitute rare earth ions into spinel ferrites due to 4f-3d couplings that enhance the structural, magnetic and electrical properties of nano ferrites [2]. The electrical and magnetic properties of ferrites depend upon the nature of ions, their distribution against the tetrahedral and octahedral ( $B$ ) sites, and their oxidation states [3]. Moreover, the physical properties of spinel nano ferrites depend on cation distribution and the

nature and the concentration of the dopant [4]. Nowadays, applications of rare earth ions are using them in the strongest and the highest performance of permanent magnet due to the stability of their magnetic properties under high sintering temperature [5]. The aim of the present work is to introduce two substituted rare earth ions to Cu/Cr nano ferrites using standard ceramic technique and to study the influence of the structural, magnetic and electrical properties on them.

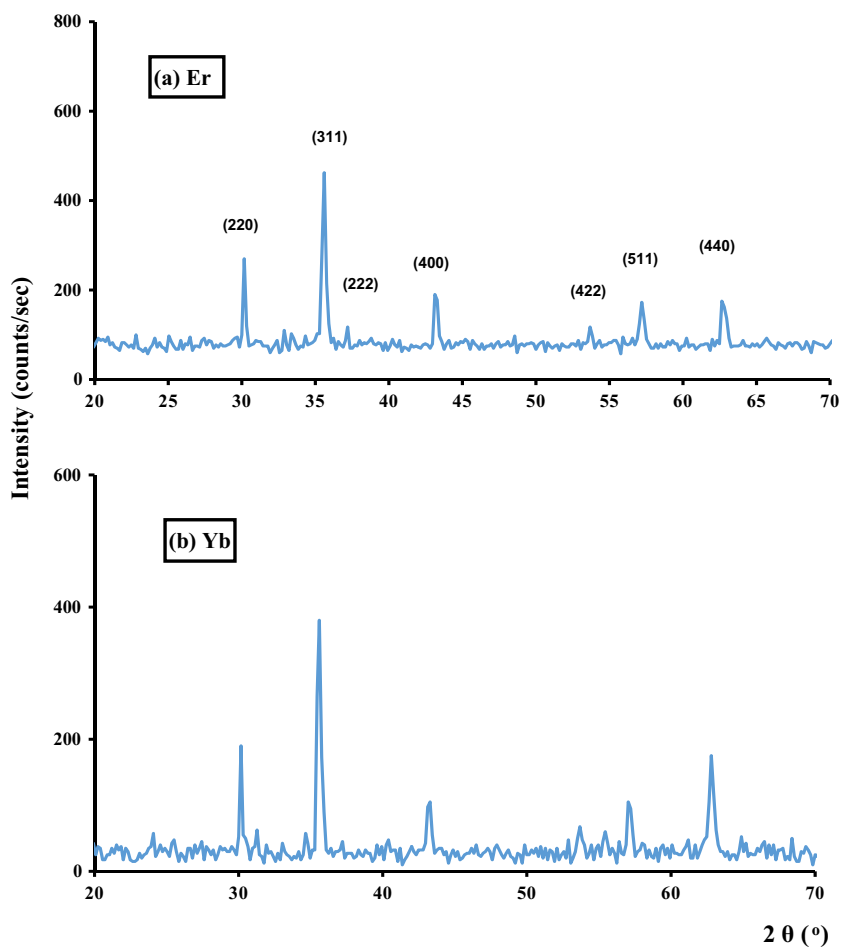
## 2 Experimental Work

$\text{CuCr}_{0.3}\text{Er}_{0.03}\text{Fe}_{1.67}\text{O}_4$  and  $\text{CuCr}_{0.3}\text{Yb}_{0.03}\text{Fe}_{1.67}\text{O}_4$  nano ferrites were prepared using standard ceramic technique [6] which is the most common one in the preparation of ferrites. The initial ingredients are copper II oxide, chromium III oxide, erbium III oxide, ytterbium III oxide and iron III oxide. Molar ratios of analar grade form oxides (BDH) were mixed together. The mixtures were ground to very fine powders using agate mortar for about 3 h; after that, the mixture was compressed into pellet form using uniaxial press under a pressure of  $5 \times 10^8 \text{N/m}^2$ . The samples were fired using Lenton furnace UAF 16/5 (England) with

✉ Asmaa A. H. El-Bassuony  
asmaa@sci.cu.edu.eg  
<http://scholar.cu.edu.eg/?q=asmaaali>

<sup>1</sup> Physics Department, Faculty of Science, Cairo University, Giza, Egypt

**Fig. 1** a, b X-ray patterns of Er and Yb samples



microprocessor to control both the rates of heating and cooling runs. Presintering was carried out at 800 °C for 6 h with a heating rate of 4 °C/min. Then, final sintering was carried out at 1000 °C for 8 h with a heating rate 4 °C/min. The samples were annealed at 1000 °C and all analyses have done at this annealed temperature.

X-ray diffraction patterns (XRD) are obtained using Diano corporation of target Cu-K $\alpha$  ( $\lambda = 1.5424 \text{ \AA}$ ). The morphology was analyzed by atomic force microscopy (AFM) using wet – SPM-9600 (scanning probe microscope) Shimadzu made in Japan, non-contact mode, scanning electron microscope for the samples using SEM Model Quanta 250 field emission gun (FEG) attached with EDX Unit (energy dispersive x-ray analyses), with accelerating voltage

30 kV, magnification  $\times 14$  up to 1,000,000 and resolution for Gun.1n), FEI company, Netherlands. Also, high-resolution transmission electron microscopy (HRTEM, Tecnai G20, FEI, Netherland) was used for the purpose of imaging, crystal structure revelation and elemental analysis qualitative and semi-quantitative analysis, model: Tecnai G20, super twin, double tilt and magnification range: up to  $\times 1,000,000$ . The room (300 K) and low (100 K) temperature magnetic hysteresis loop of the nano ferrites samples in this work were measured by maximum field 20 kG using vibrating sample magnetometer (VSM) model, Lake Shore 7410. The electrical properties were carried out by Hioki bridge Japan LCR Hi tester type 3530 (Japan) at frequencies ranging from 100 kHz to 5 MHz.

**Table 1** Values of ionic radius, crystallite size, experimental lattice parameter ( $a_{\text{exp}}$ ), theoretical lattice parameter ( $a_{\text{th}}$ ), x-ray density ( $D_x$ ), bulk density ( $D_b$ ), surface area from XRD, porosity ( $P$ ) and tolerance factor ( $T$ ) of Er and Yb samples

Samples	Ionic radius	Crystallite size (nm)	$a_{\text{exp}}$ (Å)	$a_{\text{th}}$ (Å)	$D_x$ (gm/cm <sup>3</sup> )	$D_b$ (gm/cm <sup>3</sup> )	$S$ (cm <sup>2</sup> /g) $\times 10^4$	$P$ (%)	$T$
Er	0.890	104.2	8.366	8.391	5.476	4.677	12.31	15	0.9989
Yb	0.868	100	8.362	8.390	5.488	4.360	13.76	21	0.9990

### 3 Result and Discussion

#### 3.1 X-ray Analysis

Figure 1a, b revealed that the investigated samples had single-phase cubic spinel structure and indexed by ICDD card (77-0013). The samples were accompanied by small traces of secondary phase and indexed by ICDD card (75-

0541). The calculated data estimated from XRD patterns were reported in Table 1. Both Er and Yb samples had crystallite sizes in the nanoscale range and were calculated using Debye Scherrer’s equation [7]. The lattice parameter of Yb sample was lower than that of Er sample due to the lower ionic radius and crystallite size of Yb sample than that of Er sample. The experimental lattice parameter ( $a_{exp}$ ) was in good agreement with the theoretical one which was

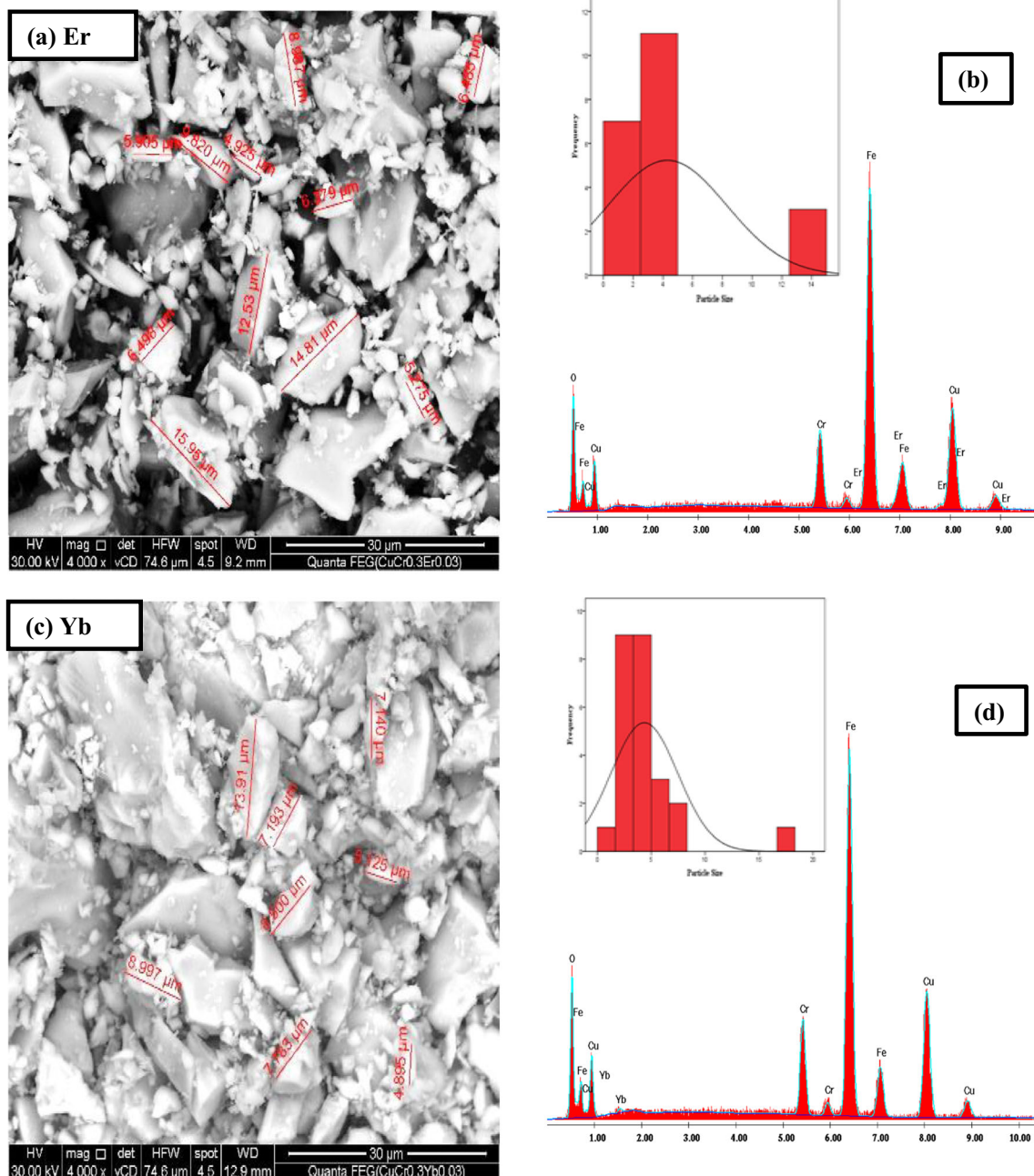
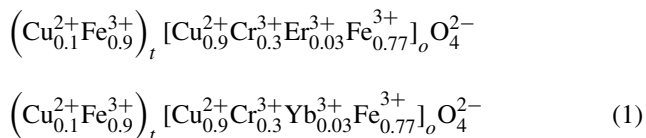


**Fig. 2** a FESEM micrograph of Er sample. b EDX pattern of Er sample (the inset is the histogram of the average particle size of Er sample). c FESEM micrograph of Yb sample. d EDX pattern of Yb sample (the inset is the histogram of the average particle size of Yb sample)

**Table 2** EDX analysis of Er and Yb samples

Element	Weight percentage (wt%)		Atomic percentage (at.%)	
	Theoretical	From EDX analysis	Theoretical	From EDX analysis
Er sample				
Cu	26.322	25.62	14.286	16.73
Cr	6.461	7.36	4.286	5.87
Er	2.079	5.66	0.429	1.40
Fe	38.630	44.91	23.857	33.36
O	26.509	16.45	57.143	42.64
Yb sample				
Cu	26.303	27.99	14.286	18.05
Cr	6.457	7.92	4.286	6.24
Yb	2.149	2.76	0.429	0.65
Fe	38.602	44.90	23.857	32.95
O	26.490	16.43	57.143	42.10

calculated using the predictable cation distribution shown as follow:



The theoretical lattice parameter is calculated from the following relation [8]:

$$a_{th} = \frac{8}{3\sqrt{3}} \left[ (r_A + R_o) + \sqrt{3} (r_B + R_o) \right] \tag{2}$$

where  $r_A$ ,  $r_B$  and  $R_o$  are ionic radii of A-site, B-site and for oxygen (1.38 Å) [9], respectively.

The x-ray density  $D_x$  was calculated using the following relation [8]:

$$D_x = \frac{ZM}{Na^3} \tag{3}$$

where  $Z$  is the number of molecules per unit cell,  $N$  is Avogadro’s number,  $M$  is the molecular weight and  $a$  is the lattice parameter of nano ferrites. In addition, the bulk density  $D_b$  was calculated using the following relation [8]:

$$D_b = \frac{m}{V} \tag{4}$$

where  $m$  is the weight of the sample and  $V$  is the volume of the sample. It is observed that, Yb sample had the highest  $D_x$  than that of Er sample; on the other hand, Er sample had the highest  $D_b$  than that of Yb sample. This may be

attributed to the lower lattice parameter of Yb sample than that of Er sample. It is known that the porosity was calculated using the formula [10]:

$$P = 1 - \frac{D_b}{D_x} \times 100\% \tag{5}$$

One can obtain that the porosity of Er sample had the lowest porosity than that of Yb sample, which improved the densification of the sample. Moreover, the tolerance factor  $T$  was suggested by the following relation [11]:

$$T = \frac{1}{\sqrt{3}} \left( \frac{r_A + R_o}{r_B + R_o} \right) + \frac{1}{\sqrt{2}} \left( \frac{R_o}{r_B + R_o} \right) \tag{6}$$

It is observed from Table 1 that the tolerance factor for both samples were closed to unity which suggested that the samples were spinel structure. In addition, the specific surface area ( $S$ ) was calculated from XRD analysis and reported in Table 1 from the following relation [12]:

$$S = \frac{6000}{\text{Particle size in nm} \times \text{bulk density}} \tag{7}$$

One can observe that the specific surface area ( $S$ ) of Yb sample was higher than that of Er sample due to the crystallite size of Yb sample was lower than that Er sample.

### 3.2 FESEM and EDX Analysis

Figure 2a–d clarified the field emission scanning electron microscopy (FESEM) and the energy-dispersive x-ray analysis

**Table 3** Values of ionic radius, crystallite size from XRD, particle size from FESEM, particle size from HRTEM, particle size from AFM and roughness of Er and Yb samples

Sample	Ionic radius (Å)	Crystallite size XRD (nm)	Particle size FESEM (µm)	Particle size HRTEM (nm)	Particle size AFM (nm)	Roughness
Er	0.890	104.2	4.30	100.84	60	1.41
Yb	0.868	100	4.36	82.41	51	1.23

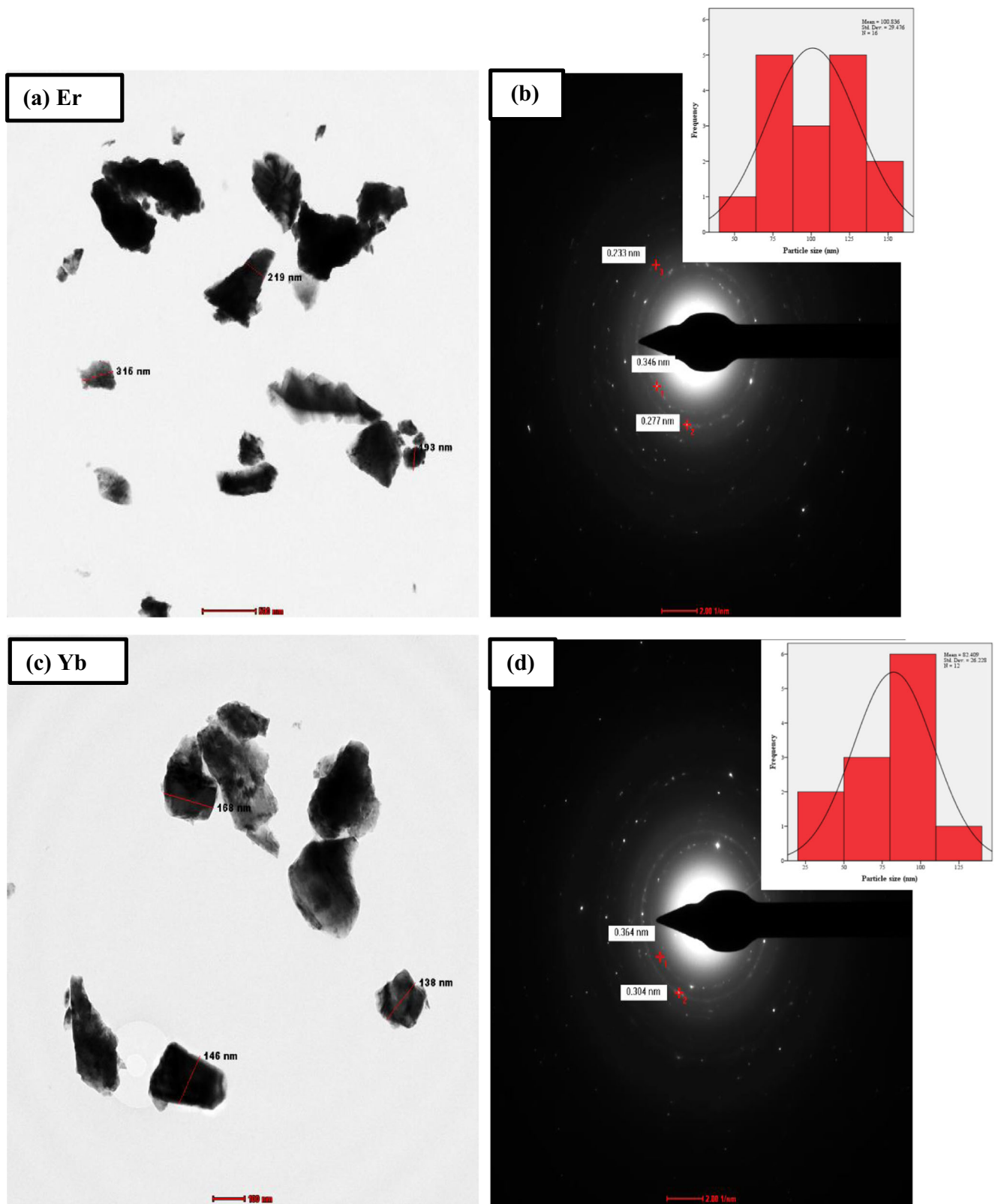


**Fig. 3** **a** HRTEM micrograph of Er sample. **b** SAED pattern of Er sample (the inset is the histogram of the average particle size of Er sample). **c** HRTEM micrograph of Yb sample. **d** SAED pattern of Yb sample (the inset is the histogram of the average particle size of Yb sample)



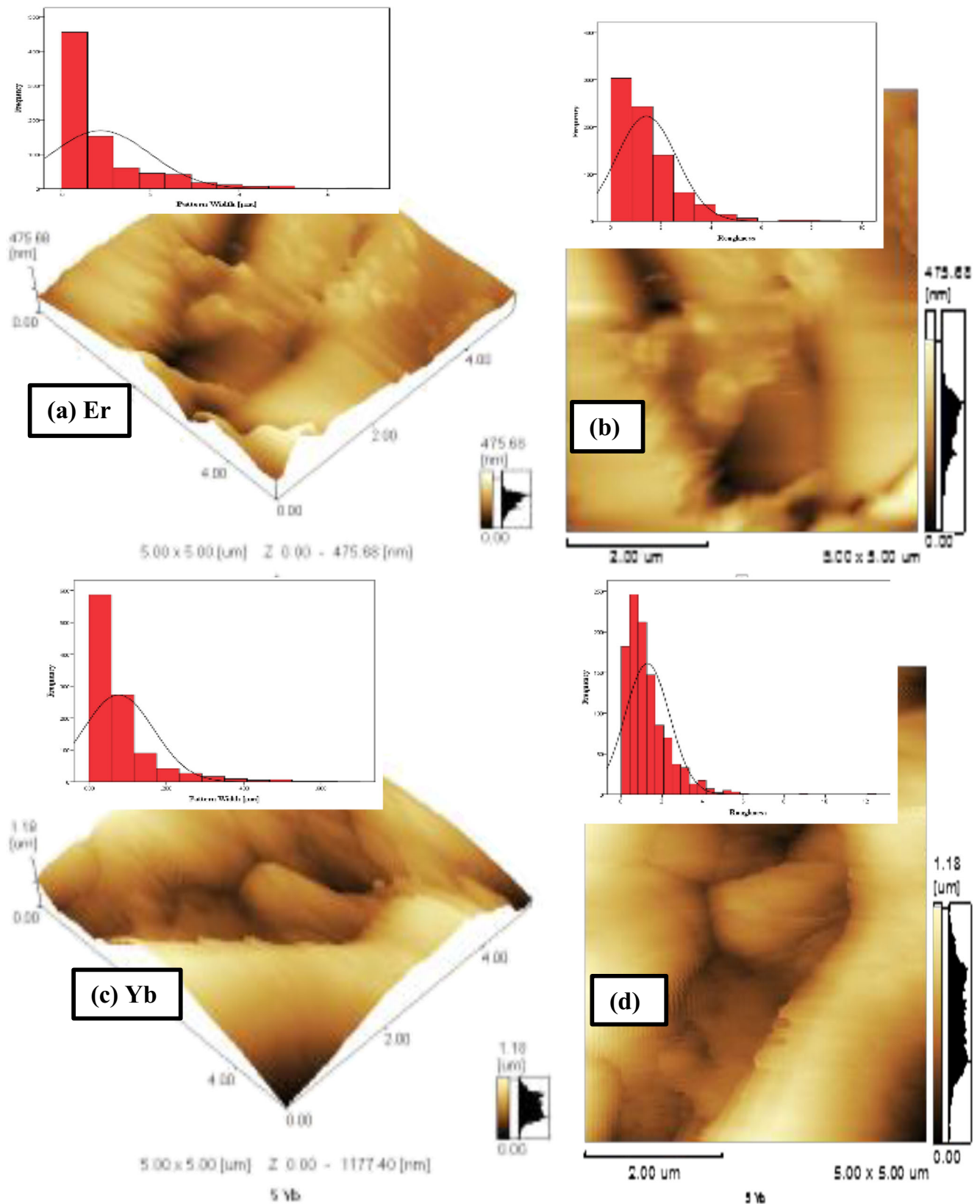


**Fig. 4** **a** 3D image AFM of Er sample (the inset is the histogram of the average particle size of Er sample). **b** Plane image AFM of Er sample (the inset is the histogram of the surface roughness of Er sample).

**c** 3D image AFM of Yb sample (the inset is the histogram of the average particle size of Yb sample). **d** Plane image AFM of Yb sample (the inset is the histogram of the surface roughness of Yb sample)

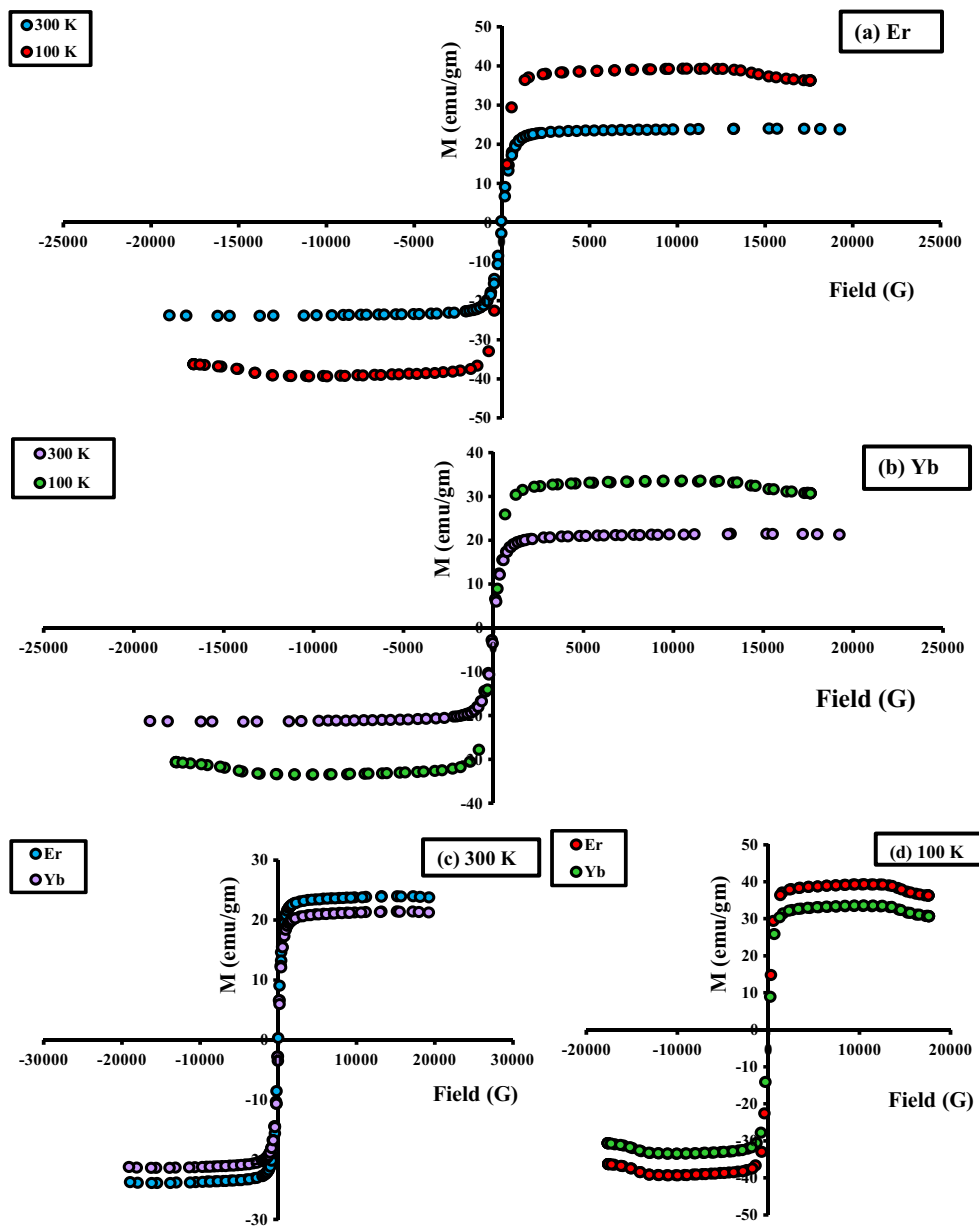


Fig. 5 a–d Magnetic hysteresis loop at room and low temperatures of Er and Yb samples

Table 4 Values of magnetic constants of Er and Yb samples

Magnetic parameters	Crystallite size (nm)	$H_c$ (G)	$M_s$ (emu/g)	$M_r$ (emulg)	Squareness $M_r/M_s$	Experimental magnetic moment (BM)	Anisotropy $k$ (erg/G)
Er sample							
300 K	104.2	26.686	23.955	1.2086	0.050	1.04	652.3
100 K		17.371	39.324	0.81821	0.021	1.70	697.0
Yb sample							
300 K	100	30.694	21.427	1.4445	0.067	0.92	671.1
100 K		21.875	33.553	0.83160	0.025	1.45	749.0

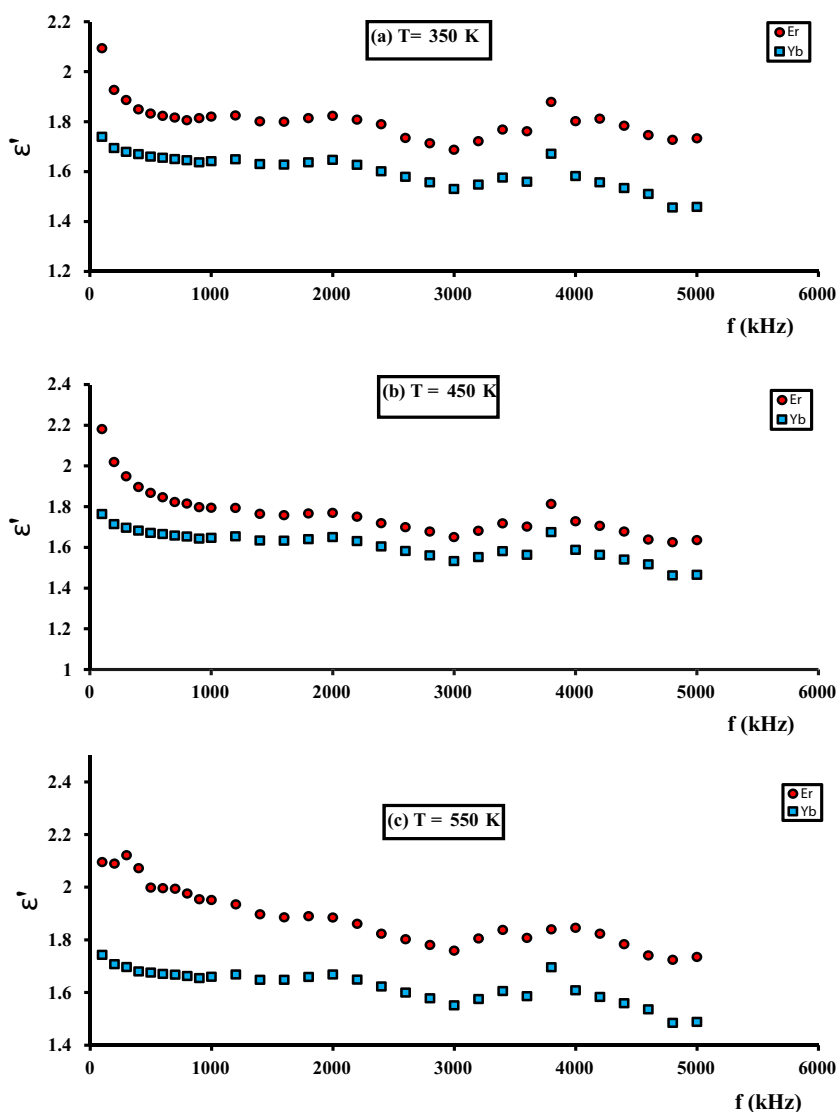
(EDX) of the investigated samples. The FESEM micrographs showed irregular distribution due to the samples had large agglomerations as in Fig. 2a, c. These agglomerations depended on many factors such as surface area, shape factor, porosity and density [13] as shown in Table 1. It is hard to estimate the particle size accurately from FESEM micrograph due to these agglomerations [14]. Figure 2b, d and Table 2 estimated the EDX for the investigated sample. The compositional analyses showed the atomic percentage (at.%) and weight percentage (wt%) of the investigated samples which were calculated theoretically and from EDX analysis and reported in Table 2. The theoretical compositional analysis was nearly in good agreement with that obtained from EDX analysis as reported in Table 2. It is observed that there was a slight difference between the theoretical (at.%) and that determined from EDX analysis due to the surface crystalline defect of the nano ferrites [15].

The inset of Fig. 2b, d showed the histogram of average particle size using ImageJ software and reported in Table 3. It is observed that the particle size of Yb sample was higher than that of Er sample due to the high agglomeration of smaller crystallite size of Yb sample.

### 3.3 HRTEM Analysis

Figure 3a–d illustrated the HRTEM of Er and Yb samples. It is observed that the morphology revealed large agglomerations due to the nanoscale size of the samples and may be due to the particle proportional to their volume [16]. The particles size reported in Table 3, assured that the sizes of the samples were in the nanoscale range. A closer look at the selected area electron diffraction pattern (SAED) of Yb sample, showed larger white spots which indicated more crystallinity of Yb sample than that of Er sample. The

**Fig. 6** a–c The dielectric constant of Er and Yb samples





histogram deduced from HRTEM analysis using ImageJ software indicated the average particle size and reported in Table 3.

### 3.4 AFM Analysis

Figure 4a–d showed the atomic force microscopy (AFM) of Er and Yb samples. The histogram of the average size and the surface roughness were inset in Fig. 4a–d in which their values were reported in Table 3. It is observed that the surface roughness of Er sample shown in Fig. 4b was larger than that of Yb sample shown in Fig. 4d. This is attributed to the higher surface activity of Er sample than that of Yb sample [17, 18]. The histogram of the particle size calculated from AFM analysis was inset in Fig. 4a, c. One can observe from the figure and Table 3 that the particle

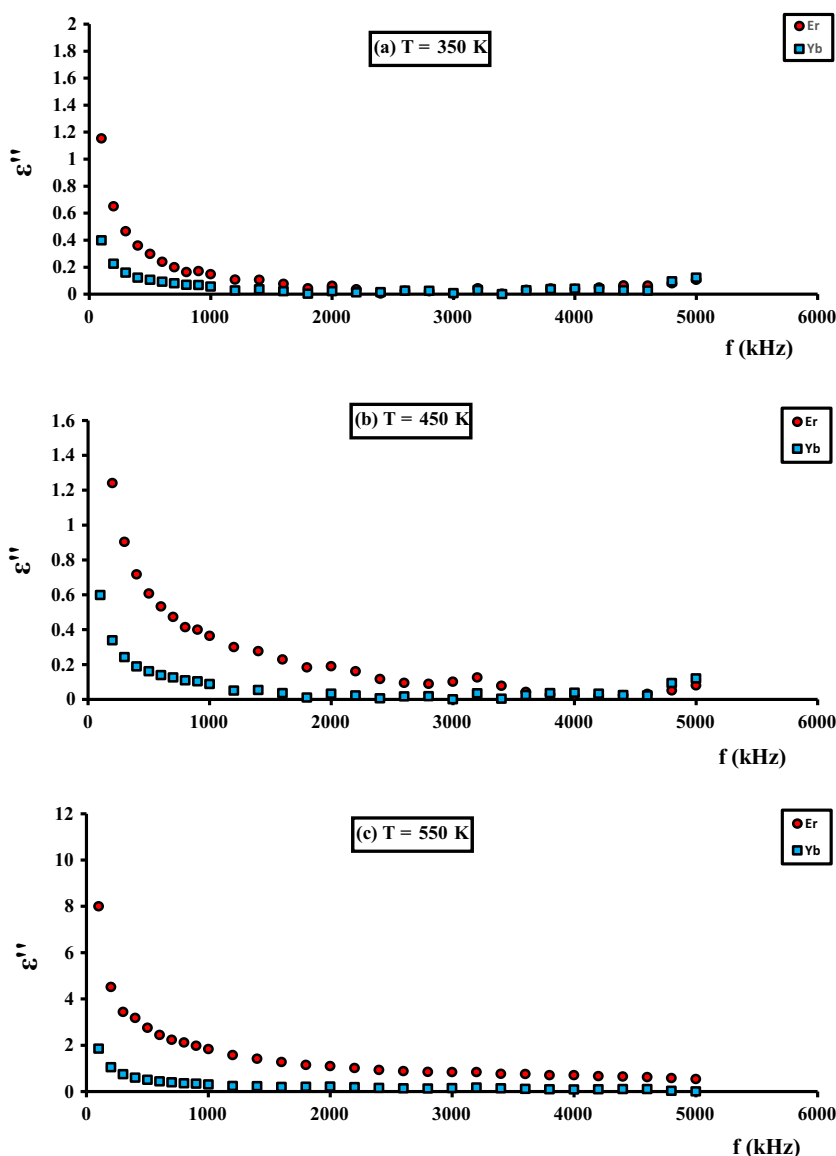
sizes of Er sample estimated from XRD, FESEM, HRTEM and AFM analyses were larger than that of Yb sample due to the larger ionic radius of Er ion than that of Yb ion.

### 3.5 Magnetic Properties

Figure 5a–d displayed the magnetic hysteresis loop at room (300 K) and at low (100 K) temperatures for Er and Yb samples. All samples showed ferromagnetic behaviour and behaved as semiconductors like [19]. The obtained data calculated from magnetic hysteresis loop were reported in Table 4. The experimental magnetic moment was given by the following equation [20]:

$$\eta = \frac{Mwt \times M_s}{5585} \tag{8}$$

Fig. 7 a–c The dielectric loss of Er and Yb samples



The saturation magnetization ( $M_s$ ) increased at low temperature (100 K) than that at room temperature (300 K) due to the experimental magnetic moment increased at 100 K than that at 300 K. However, the coercivity ( $H_c$ ) and remnant magnetization ( $M_r$ ) decreased at 100 K than that at 300 K. This may be attributed to the variation of the coercive field with rare earth type was ascribed to the frequency shift of vibrational modes and was explained on the basis of the changes in magnetocrystalline anisotropy [20]. The magnetocrystalline anisotropy constant ( $k$ ) is calculated [20] and reported in Table 4. It is observed that the magnetocrystalline anisotropy constant ( $k$ ) at 100 K was higher than that at 300 K which revealed that the samples may have technological magnetic applications at low temperature.

It is known that the squareness of spinel ferrite varies from 0 to 1 [21]. Hence, the particles interact by magnetostatic interaction happened when the squareness  $< 0.5$ , while for random oriented non-interact particles happened when

the squareness = 0.5. Also, when  $0.5 < \text{squareness} < 1$ , it suggested the existence of the exchange coupling particles. Therefore, the squareness of the investigated samples reported in Table 4, had squareness  $< 0.5$  which attributed to the magnetostatic interactions.

### 3.6 Electrical Properties

Figures 6, 7 and 8a–c illustrated the variation of dielectric constant ( $\epsilon'$ ), dielectric loss ( $\epsilon''$ ) and dielectric loss tangent ( $\tan \delta$ ) for all the investigated samples at different temperatures (350, 450 and 550 K). At lower frequency range ( $\epsilon'$ ,  $\epsilon''$  and  $\tan \delta$ ) showed a rapid dispersion due to the interfacial polarization. At higher frequency range, the dispersion had nearly frequency independent response due to the rotational displacements of the dipoles which resulted in the orientational polarization [22]. As the temperature increased, the  $\epsilon'$ ,  $\epsilon''$  and  $\tan \delta$  increased. However, they

**Fig. 8** a–c The dielectric loss tangent of Er and Yb samples

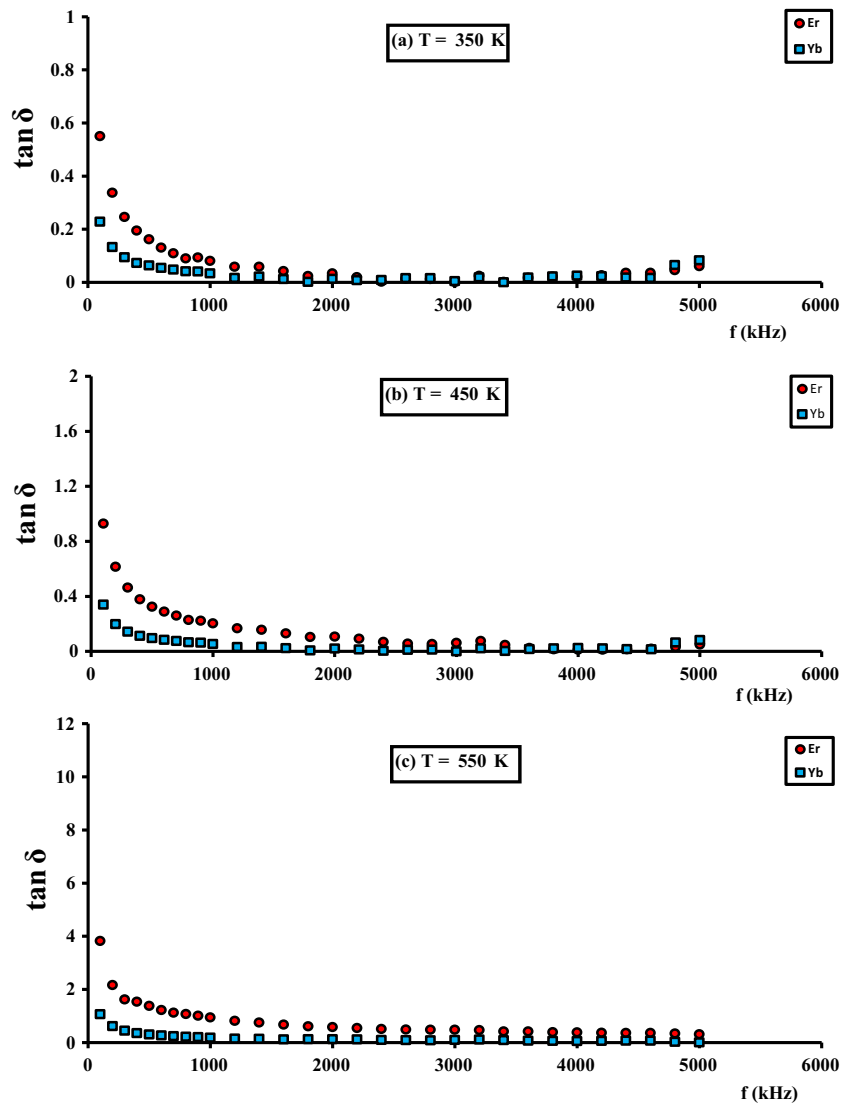
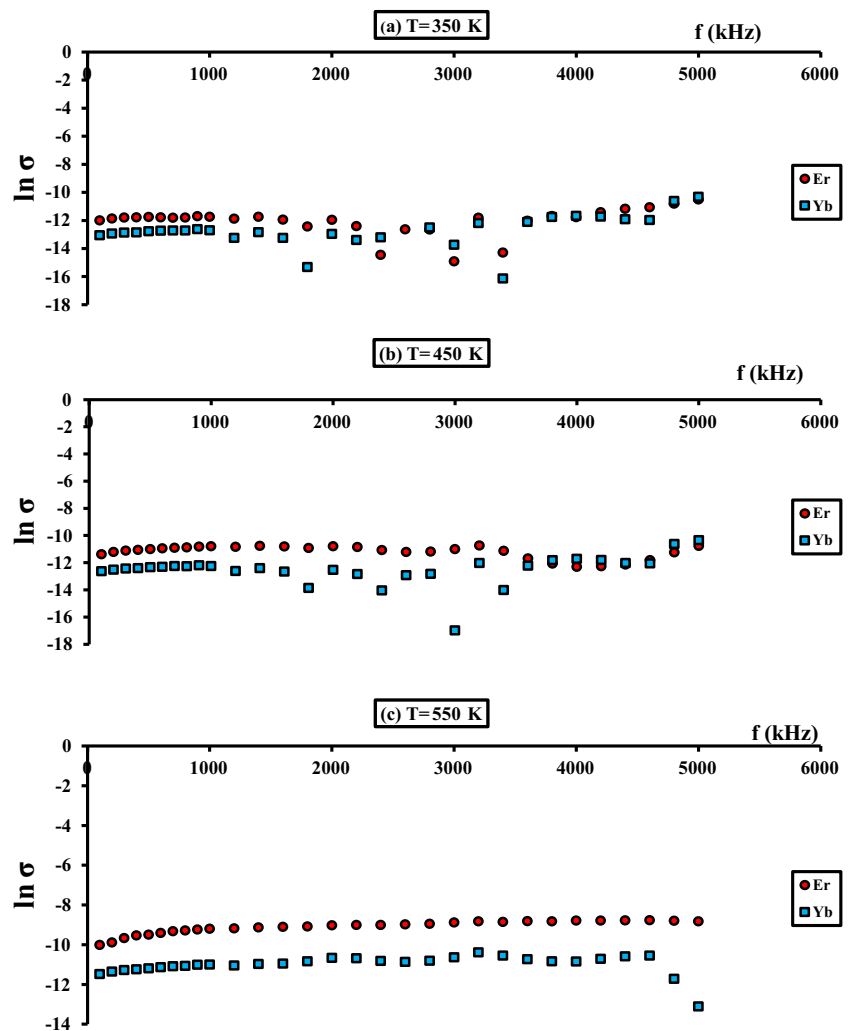


**Fig. 9** a–c The ac conductivity of Er and Yb samples



decreased with the increasing of the frequency and this was the normal behaviour for semiconducting ferrites [23].

Figure 9a–c showed the variation of the ac conductivity ( $\sigma_{ac}$ ) against the frequency of Er and Yb samples. It is observed that at low-frequency region, the ac conductivity ( $\sigma_{ac}$ ) remained constant; however, at high-frequency region, the ac conductivity ( $\sigma_{ac}$ ) increased. This increase may be attributed to the increase of hopping of charge carriers between the ions of  $\text{Fe}^{2+} \leftrightarrow \text{Fe}^{3+}$  and  $\text{Er}^{3+} \leftrightarrow \text{Er}^{2+}$  or  $\text{Yb}^{3+} \leftrightarrow \text{Yb}^{2+}$ , thereby the conduction of such ferrite was increased [24]. As the temperature increased, the conductivity decreased which estimated that the samples gave high resistivity at 550 K.

## 4 Conclusion

1. X-ray analysis confirmed that all samples had cubic spinel structures.
2. The morphology assured that the samples were in the nanoscale range.

3. Er sample had higher ( $M_s$ ) and lower ( $H_c$ ) than that of Yb sample suggesting Er sample can be applied in magnetic applications.
4. Yb sample had higher resistivity and low dielectric loss than that of Er sample suggesting Yb sample can be applied in electrical applications.

## References

1. Zaki, H.M., Al-Heniti, S.: J. Nanosci. Nanotechnol. **12**, 7126 (2012)
2. Yu, M., Draskovic, T.I., Wu, Y.: Cu(I)-based delafossite compounds as photocathodes in p-type dye-sensitized solar cells. Phys. Chem. Chem. Phys. **16**, 5026–5033 (2014). <https://doi.org/10.1039/c3cp55457k>
3. Maklad, M.H., Shash, N.M., Abdelsalam, H.K.: Synthesis, characterization and magnetic properties of nanocrystalline. Int. J. Mod. Phys. B **28**(25), 1450165 (2014). <https://doi.org/10.1142/S0217979214501653>
4. Hong, B.C., Kawano, K.: Luminescence studies of the rare earth ions-doped  $\text{CaF}_2$  and  $\text{MgF}_2$  films for wavelength conversion. J. Alloys Compd. **408–412**, 838–841 (2006). <https://doi.org/10.1016/j.jallcom.2005.01.133>

5. Maklad, M.H., Shash, N.M., Abdelsalam, H.K.: Structural and magnetic properties of nanograined Ni<sub>0.7-y</sub>Zn<sub>0.3</sub>Ca<sub>y</sub>Fe<sub>2</sub>O<sub>4</sub> spinels Structural and magnetic properties of nanograined. *Eur. Phys. J. Appl. Phys.* **66**, 30402 (2014). <https://doi.org/10.1051/epjap/2014130573>
6. El-Bassuony, A.A.H.: Tuning the Structural and Magnetic Properties on Cu/Cr Nanoferrite Using Different Rare-Earth Ions. *Journal of Materials Science, Materials in Electronics* (2017)
7. El-Bassuony, A.A.H., Abdelsalam, H.K.: Modification of AgFeO<sub>2</sub> by double nanometric delafossite to be suitable as energy storage in solar cell. *J. Alloys Compd.* **726**(2017), 1106–1118 (2017). <https://doi.org/10.1016/j.jallcom.2017.08.087>
8. Krishna, K.R., Ravinder, D., Kumar, K.V., Lincon, C.A.: Synthesis, XRD & SEM studies of zinc substitution in nickel ferrites by citrate gel technique. *World J. Condens. Matter Phys.* **2**, 153–159 (2012)
9. Shannon, R.D.: Revised effective ionic radii and systematic studies of interatomic distances in halides and chalcogenides. *Acta Crystallogr. Sect. A.* **32**, 751–767 (1976). <https://doi.org/10.1107/S0567739476001551>
10. Bamzai, K.K., Kour, G., Kaur, B., Kulkarni, S.D.: *J. Magn. Magn. Mater.* **327**, 159 (2013)
11. Desai, P.A., Athawale, A.A.: Microwave combustion synthesis of silver doped lanthanum ferrite magnetic nanoparticles. *Def. Sci. J.* **63**, 285–291 (2013). <https://doi.org/10.14429/dsj.63.2387>
12. Zhang, D.-H., Li, H.-B., Li, G.-D., Chen, J.-S.: Magnetically recyclable Ag-ferrite catalysts: general synthesis and support effects in the epoxidation of styrene. *Dalton Trans.* (2009)
13. Ateia, E., El, A.A.H.: Fascinating improvement in physical properties of Cd/Co nanoferrites using different rare earth ions. *J. Mater. Sci. Mater. Electron.* **28**, 11482–11490 (2017). <https://doi.org/10.1007/s10854-017-6944-0>
14. Tholkappian, R., Vishista, K.: *Phys. B Condens. Matter* **448**, 177 (2014)
15. Deraz, N.M., Alarifi, A.: Microstructure and magnetic studies of zinc ferrite nano-particles. *Int. J. Electrochem. Sci.* **7**, 6501–6511 (2012)
16. Ahmad, I., Abbas, T., Ziya, A.B., Maqsood, A.: Structural and magnetic properties of erbium doped nanocrystalline Li – Ni ferrites. *Ceram. Int.* **40**, 7941–7945 (2014). <https://doi.org/10.1016/j.ceramint.2013.12.142>
17. Ateia, E., Salah, L.M., El-Bassuony, A.A.H.: Investigation of cation distribution and microstructure of nano ferrites prepared by different wet methods. *J. Inorg. Organomet. Polym. Mater.* **25**, 1362–1372 (2015). <https://doi.org/10.1007/s10904-015-0248-8>
18. Rajesh, D., Sunandana, C.S.: XRD, optical and AFM studies on pristine and partially iodized Ag thin film. *Results Phys.* **2**, 22 (2012)
19. Zhou, X., Jiang, J., Li, L., Xu, F.: Preparation and magnetic properties of La-substituted Zn-Cu-Cr ferrites via a rheological phase reaction method. *J. Magn. Magn. Mater.* **314**, 7–10 (2007). <https://doi.org/10.1016/j.jmmm.2007.02.030>
20. El-Bassuony, A.A.H., Abdelsalam, H.K.: Giant exchange bias of hysteresis loops on Cr<sup>3+</sup>-doped Ag Nanoparticles. *J. Supercond. Nov. Magn.* (2017)
21. Ateia, E.E., El-Bassuony, A.A., Abdelatif, G., Soliman, F.S.: Novelty characterization and enhancement of magnetic properties of Co and Cu nanoferrites. *J. Mater. Sci. Mater. Electron.* **28**, 11482–11490 (2017). <https://doi.org/10.1007/s10854-016-5517-y>
22. Gabal, M.A., Al Angari, Y.M.: Low-temperature synthesis of nanocrystalline NiCuZn ferrite and the effect of Cr substitution on its electrical properties. *J. Magn. Magn. Mater.* **322**, 3159–3165 (2010). <https://doi.org/10.1016/j.jmmm.2010.05.054>
23. El-Bassuony, A.A.: Enhancement of structural and electrical properties of novelty nanoferrite materials. *J. Mater. Sci. Mater. Electron.* **28**, 14489–14498 (2017). <https://doi.org/10.1007/s10854-017-7312-9>
24. Ravinder, D., Reddy, K.S., Mahesh, P., Rao, T.B., Venudhar, Y.C.: Electrical conductivity of chromium substituted copper ferrites. *J. Alloys Compd.* **370**, 17–22 (2004). <https://doi.org/10.1016/j.jallcom.2003.09.126>